inorganics

MDPI

Article

Reaching the Maximal Unquenched Orbital Angular Momentum L = 3 in Mononuclear Transition-Metal Complexes: Where, When and How?

Vladimir S. Mironov [1,2]

[1] Shubnikov Institute of Crystallography of Federal Scientific Research Centre "Crystallography and Photonics" of Russian Academy of Sciences, Leninskiy Prospekt 59, Moscow 119333, Russia; mirsa@list.ru
[2] Institute of Problems of Chemical Physics, IPCP RAS, Chernogolovka 142432, Russia

Abstract: The conditions for achieving the maximal unquenched orbital angular momentum L = 3 and the highest magnetic anisotropy in mononuclear 3d complexes with axial coordination symmetry are examined in terms of the ligand field theory. It is shown that, apart from the known linear two-coordinate $3d^7$ complex $Co^{II}(C(SiMe_2ONaph)_3)_2$ characterized by record magnetic anisotropy and single-molecule magnet (SMM) performance (with the largest known spin-reversal barrier U_{eff} = 450 cm^{-1}), the maximal orbital angular momentum L = 3 can also be obtained in linear two-coordinate $3d^2$ complexes (V^{3+}, Cr^{4+}) and in trigonal-prismatic $3d^3$ (Cr^{3+}, Mn^{4+}) and $3d^8$ (Co^+, Ni^{2+}) complexes. A comparative assessment of the SMM performance of the $3d^2$, $3d^3$ and $3d^8$ complexes indicates that they are unlikely to compete with the record linear complex $Co^{II}(C(SiMe_2ONaph)_3)_2$, whose magnetic anisotropy is close to the physical limit for a 3d metal.

Keywords: magnetic anisotropy; single-molecule magnet; unquenched orbital momentum; spin-reversal barrier; mononuclear 3d complexes; spin-orbit coupling

check for updates

Citation: Mironov, V.S. Reaching the Maximal Unquenched Orbital Angular Momentum L = 3 in Mononuclear Transition-Metal Complexes: Where, When and How? *Inorganics* **2022**, *10*, 227. https://doi.org/10.3390/inorganics10120227

Academic Editor: Peter Segl'a

Received: 28 October 2022
Accepted: 24 November 2022
Published: 27 November 2022

1. Introduction

Mononuclear paramagnetic metal complexes with high magnetic anisotropy are of great interest in recent years, largely due to the development of low-dimensional molecule-based magnetically bistable materials featuring slow magnetic relaxation and blocking of magnetization at low temperature—single-molecule magnets (0D, SMMs) [1–9] and single-chain magnets (1D, SCMs) [10–12]. The overall performance of SMMs and SCMs is quantified by two key parameters, the effective energy barrier to magnetization reversal (U_{eff}) and the blocking temperature (T_B), below which the magnetization persists in zero external fields [6–12]. The U_{eff} and T_B values depend strongly on the magnetic anisotropy of spin carriers incorporated in the high-spin molecule. The early research was mainly focused on polynuclear transition-metal complexes based on high-spin 3d-ions with enhanced single-ion magnetic anisotropy arising from the zero-field splitting (ZFS) of the ground spin state, such as Mn^{3+} and Ni^{2+} [1–3]. Then, after the discovery of slow magnetic relaxation in mononuclear lanthanide complexes (2003) [13] and later in mononuclear transition metal compounds (2010) [14,15], research interest has turned to SMMs involving single paramagnetic ion with high magnetic anisotropy due to the first-order unquenched orbital angular momentum, 4f-complexes [16–24] and special orbitally degenerate 3d-complexes with high axial symmetry [25,26]. These mononuclear 4f- and 3d-SMMs are known as single-ion magnets (SIMs).

At present, it is generally recognized that the unquenched orbital angular momentum of the magnetic metal ions is the most important factor governing large magnetic anisotropy and high SMM characteristics [8]. In this respect, lanthanide ions are especially attractive. In fact, all Ln^{3+} ions with open $4f^N$-shell exhibit large unquenched orbital angular momentum L (ranging from 3 to 6, except Gd^{3+} with L = 0) due to very weak ligand-field (LF) splitting

energy and strong spin-orbit coupling (SOC) of 4f-electrons; the maximal orbital momentum $L = 6$ occurs in Nd^{3+} ($4f^3$, $^4I_{9/2}$), Pm^{3+} ($4f^4$, $^5I_4$), Ho^{3+} ($4f^{10}$, $^5I_8$) and Er^{3+} ($4f^{11}$, $^4I_{15/2}$) ions. Due to the strong SOC of 4f electrons, the orbital momentum L and spin S are coupled into the total angular momentum J; the ground state of free $Ln^{3+}(4f^N)$ ions corresponds to the $^{2S+1}L_J$ multiplet with $J = L - S$ ($N < 7$) and $J = L + S$ ($N > 7$). For Ln^{3+} ions in a ligands coordination environment, the ground J-multiplet undergoes LF splitting into $2J + 1$ sublevels (called Stark sublevels) creating a highly anisotropic ground state [8,20]. In particular, pure Ising-type uniaxial magnetic anisotropy occurs in monometallic lanthanide complexes with distinct axial symmetry, in which axial LF lifts the $(2J + 1)$-fold degeneracy of the ground multiplet into $\pm M_J$ microstates with a definite projection of the total angular momentum [16–24]. The energy splitting diagram of $\pm M_J$ states (E vs. M_J) depends on both the strength and the intrinsic structure of the axial LF, which is specified by three axial LF parameters B_{20}, B_{40}, B_{60} [27]. In the optimal case, the strong field stabilizes the doubly degenerate ground state with maximal M_J projection ($M_J = \pm J$) and with large energy separation from excited LF states thereby resulting in a double-well potential with the high-energy barrier U_{eff} inherent to high-performance SMMs. In particular, such LF-splitting pattern is observed in square antiprismatic [13], pentagonal-bipyramidal [28,29] and quasi-linear metallocene lanthanide complexes [30,31], many of which exhibit exceptionally high U_{eff} and T_B values, including a record-setting dysprosium metallocene SMM with $U_{\text{eff}} = 1541\ \text{cm}^{-1}$ and $T_B = 80$ K [31]. Recent trends in high-performance 4f SIM are reviewed in ref. [32].

Later on, since the report on the first mononuclear trigonal pyramidal Fe^{II} complexes with SMM behavior (2010) [14,15], extensive efforts have been taken to the development of 3d SIMs using diverse approaches to increase magnetic anisotropy and energy barrier; numerous 3d SIMs were reported in the past decade [8,25,26]. However, in contrast to f-block element complexes, in transition metal complexes the orbital angular momentum is commonly quenched ($L = 0$) by a strong LF to produce the spin-only ground state with low second-order magnetic anisotropy [33]. In the majority of high-spin 3d complexes, magnetic anisotropy is typically due to zero-field splitting (ZFS) of the ground spin multiplet $2S + 1$, which is generally a weak effect resulting from second-order SOC [34]. Hence, the barriers U_{eff} of 3d SIMs are mostly low, within a few tens of cm^{-1} [8,25,26,33]. The most efficient strategy toward high-performance 3d SIMs takes advantage of unquenched orbital angular momentum ($L \neq 0$) giving rise to the first-order spin-orbit splitting of the ground spin stated with $L \neq 0$, which provides considerably stronger magnetic anisotropy and high energy barriers [16–24]. Unquenched first-order orbital angular momentum can only appear in orbitally degenerate transition metal complexes with high symmetry, such as octahedral Co^{II} and $[Fe^{III}(CN)_6]^3$ complexes (O_h) [33,34], trigonal-pyramidal (C_{3v}), [14,15] trigonal-bipyramidal (D_{3h}), [35] trigonal-prismatic (D_{3h}) [36,37], pentagonal-bipyramidal (D_{5h}) [38] and linear ($D_{\infty h}$) two-coordinate complexes [39–43].

However, apart from unquenched orbital angular momentum, another important condition for the highest SMM performance of mononuclear 3d complexes is the axial limit of the magnetic anisotropy, which has a purely Ising-type nature, with zero transverse components. This case occurs in the LF of axial symmetry, which is produced by tuning the geometric axiality of the ligand environment of the 3d-ion. Depending on the specific type of the coordination polyhedron and electronic configuration of the 3d ion, the axial LF may stabilize the ground orbital doublet with the projection of the orbital angular momentum $M_L = 0, \pm 1, \pm 2$, or ± 3. The latter is further split by the first-order SOC into energy levels $\pm M_J$ with definite projection M_J of the total angular momentum J along the magnetic axis, which ranges from $L + S$ to $|L - S|$. In this regime, spin energy levels are represented by pure $|\pm M_J>$ spin wave functions, in which quantum tunneling of magnetization (QTM) is suppressed both in the ground and exited spin states. In these systems the barrier U_{eff} is controlled by the first-order SOC energy $\zeta_{3d}\boldsymbol{LS}$, which is proportional to the value of the ground-state orbital angular momentum M_L; approximately, U_{eff} is specified by $\zeta_{3d}M_L/2S$, which is the energy separation between the ground $\pm M_J$ and first exited

$\pm(M_J - 1)$ states [42]. This leads to a pure Ising magnetic anisotropy and double-well potential with two lowest $M_J = \pm J$ states similar to those in 4f SIMs [16–24]. Accordingly, the highest barriers U_{eff} are observed in 3d SIMs with large orbital momentum M_L, namely, in linear $3d^7$ complexes $[Fe^{I}(C(SiMe_3)_3)_2]^-$ (226 cm^{-1}) [40] and [(sIPr)Co^{II}NDmp] (413 cm^{-1}) [41] and also in trigonal-prismatic Co^{II} complex (152 cm^{-1}) [36] featuring $L = 2$, $S = 3/2$ and $M_J = \pm 7/2$ in the ground state. The record barrier belongs to linear two-coordinate cobalt complex, $Co^{II}(C(SiMe_2ONaph)_3)_2$ (U_{eff} = 450 cm^{-1}) [42] and for the monocoordinated cobalt(II) adatom on a MgO surface (U_{eff} = 468 cm^{-1}) [43] which have $L = 3$, $S = 3/2$ and $M_J = \pm 9/2$ in the ground state.

Considering that a large unquenched orbital angular momentum is extremely important for attaining the highest SMM performance in 3d-SIMs, the relevant question is in which mononuclear 3d complexes, besides the already known record-breaking linear two-coordinate $3d^7$ complexes [42,43], the maximum orbital angular momentum $L = 3$ (represented by the ground orbital doublet $M_L = \pm 3$) is feasible. In this paper, general conditions for the appearance of the maximum orbital angular momentum $L = 3$ in mononuclear 3d complexes are analyzed in terms of the LF theory. We show that, apart from the linear two-coordinate $3d^7$ complex $Co^{II}(C(SiMe_2ONaph)_3)_2$ [42], the ground-state orbital doublet $M_L = \pm 3$ can occur in linear $3d^2$ complexes and in trigonal-prismatic $3d^3$ and $3d^8$ complexes. Specific conditions for the LF splitting pattern of 3d orbitals leading to $L = 3$ are established.

2. Results

Below, the basic conditions for the realization of the maximal orbital angular momentum $M_L = \pm 3$ in mononuclear 3d complexes with the axial LF are analyzed. First of all, it is clear that the ground orbital doublet $M_L = \pm 3$ can only occur in 3d ions, which in the free-ion state have a ^{2S+1}F ground atomic term featuring the maximum orbital angular momentum $L = 3$ for 3d ions, i.e., $3d^2$, $3d^3$, $3d^7$ and $3d^8$ ions. In transition–metal complexes with the LF of axial symmetry, the lowest ^{2S+1}F term splits into four orbital components $^{2S+1}F(M_L)$ with a projection of orbital momentum $M_L = 0, \pm 1, \pm 2, \pm 3$ (Figure 1). The objective of the present study is to establish conditions for the $M_L = \pm 3$ orbital doublet to be the ground state.

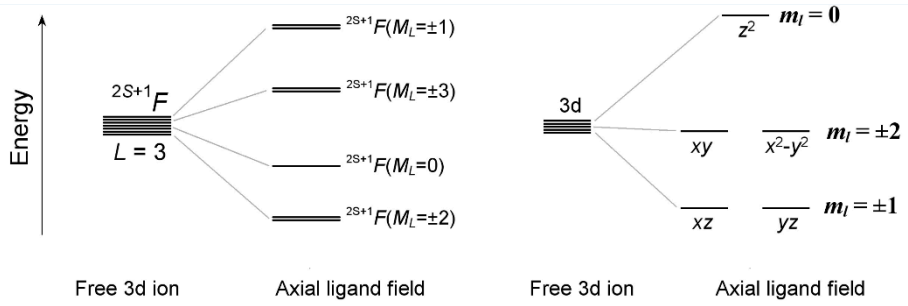

Figure 1. Energy splitting of the ground-state atomic term $^{2S+1}F(L = 3)$ and 3d orbitals in a ligand field of axial symmetry. The orbital composition of the $^{2S+1}F(M_L = \pm 3)$ states is shown below in the insets to the corresponding figures.

In an axial LF, five 3d orbitals are split into three groups of orbitals with a definite projection of the one-electron orbital angular momentum m_l on the anisotropy axis z, $3d_{z2}$ ($m_l = 0$), ($3d_{xz}$, $3d_{yz}$) ($m_l = \pm 1$) and $3d_{xy}$, $3d_{x2-y2}$ ($m_l = \pm 2$) (Figure 1). A necessary (but not sufficient) condition for the $M_L = \pm 3$ ground state is the presence of one unpaired electron in each of the two doubly degenerate 3d orbitals with magnetic numbers $m_l = \pm 1$, and $m_l = \pm 2$, i.e., $(xz, yz)^1(xy, x2 - y2)^1$ or $(xz, yz)^3(xy, x2 - y2)^3$. For each of the 3d ions selected above, the LF splitting pattern of 3d-orbitals leading to the $^{2S+1}F(M_L = \pm 3)$ ground state is examined in terms of the conventional LF theory, which takes into account the interelectron repulsion (quantified in terms of the Racah parameters B and C) and SOC, $\zeta_{3d}\Sigma_i \boldsymbol{l}_i \boldsymbol{s}_i$. LF

calculations are performed with the full basis set of $3d^N$ configurations involving 45 ($3d^2$, $3d^8$) and 120 ($3d^3$, $3d^7$) $|LM_LSM_S>$ microstates. Details of LF calculations are available in the Supplementary Materials.

2.1. $3d^2$ Complexes (V^{3+}, Cr^{4+})

The necessary condition for the $^3F(M_L = \pm 3)$ orbital doublet to be the ground state is to have the LF spitting pattern $E(z^2) > E(xz, yz) > E(xy, x2 - y2)$. Such an orbital energy scheme can occur in complexes with linear or quasi-linear two-coordinate complexes [44] similar to the quasi-linear Fe^{II} [39] and Co^{II} complexes [42]. For a quantitative evaluation, LF calculations for the energy levels of the $3d^2$ configuration were performed using the Racah parameters B = 600, C = 2900 cm^{-1} and SOC constant ζ = 150 cm^{-1}, which are typical for V^{3+} ion [45]. The calculations were performed with fixed orbital energies $E(z^2)$ = 10,000 cm^{-1}, $E(xy, x2 - y2) = 0$ and variable orbital energy $E(xz, yz) = \Delta$ (see inset in Figure 2a). The orbital doublet $^3F(M_L = \pm 3)$ (shown in the solid red line in Figure 2a) is found to be the ground state in the energy range $0 \leq \Delta \leq 5400$ cm^{-1}; at larger energies, the ground state is the orbital singlet $^3F(M_L = 0)$, whose wave function $Det||xy\uparrow, x2 - y2\uparrow||$ corresponds to two singly occupied xy and $x2 - y2$ orbitals with parallel electron spins (Figure 2a). From the point of view of coordination geometry, the only suitable case for the $^3F(M_L = \pm 3)$ ground state is a linear two-coordination of $3d^2$ ion. Numerous 3d complexes of this type were reported in the literature, as outlined in a review article [44].

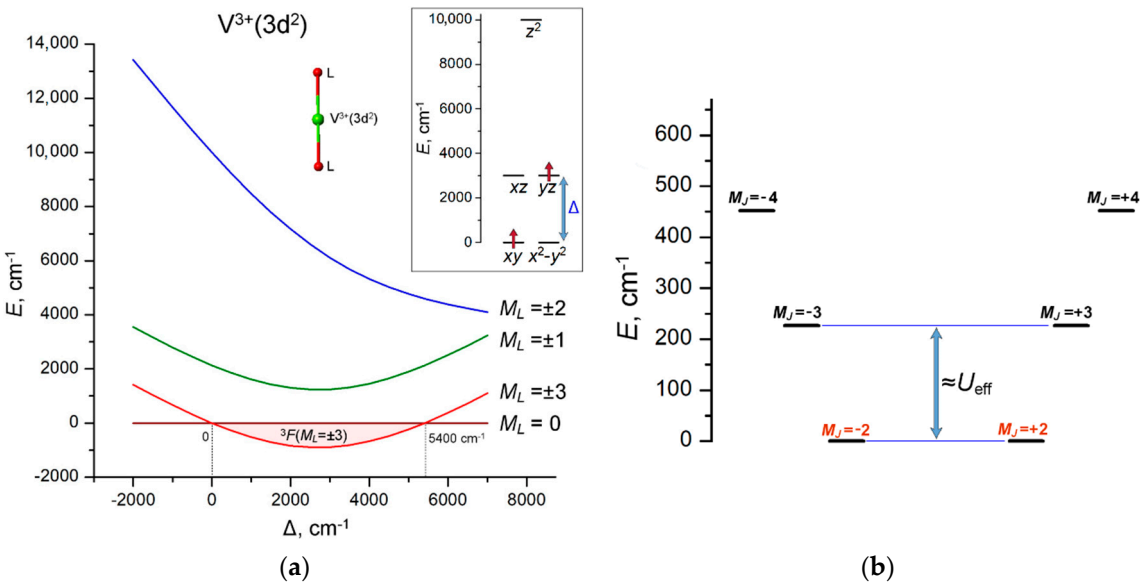

Figure 2. (**a**) Variation of the energies of the $^3F(M_L)$ LF states of $V^{3+}(3d^2)$ ion in linear coordination with increasing energy separation $\Delta = E(xz, yz) - E(xy, x2 - y2)$ between the lowest and first excited sets of 3d orbitals. The range of the stabilization of the $^3F(M_L = \pm 3)$ ground state ($0 \leq \Delta \leq 5400$ cm^{-1}) is marked with light pink. Inset: the LF splitting pattern of 3d orbitals in a linear two-coordination, $E(xy, x2 - y2) = 0$, $E(z^2)$ = 10,000 cm^{-1} (fixed) and $E(xz, yz) = \Delta$ (variable); (**b**) E vs. M_J diagram calculated at Δ = 3000 cm^{-1}. The spin-reversal barrier $U_{eff} \approx 200$ cm^{-1} is approximately estimated by the energy separation between the ground $M_J = \pm 2$ and the first excited $M_J = \pm 3$ states.

The calculated E vs. M_J diagram indicates that such a $3d^2$ complex may be a SMM with a barrier U_{eff} of about 200 cm^{-1}, as estimated from the energy gap between ground $M_J = \pm 2$ and first excited $M_J = \pm 3$ states (Figure 2b). Remarkably, the E vs. M_J diagram has an inverse order of $\pm M_J$ levels compared to the usual double-well spin energy profile (with the maximum M_J at the bottom and the minimum M_J at the top) due to the antiparallel coupling of the orbital momentum L = 3 and spin S = 1 of $V^{3+}(3d^2)$ ion. However, the actual SMM performance of the linear two-coordinate complex of V^{3+} is expected to be

much lower due to the non-Kramers nature of the ground doublet $M_J = \pm 2$, which is subject to splitting due to possible deviations from the axiality of the molecular structure, leading to fast under-barrier quantum tunneling of magnetization (QTM) that shortcuts the energy barrier. Hence, in terms of SMM performance, the situation with the linear two-coordinate $3d^2$ complex is much less favorable compared to the record cobalt $3d^7$ complex $Co^{II}(C(SiMe_2ONaph)_3)_2$ [42].

2.2. $3d^3$ Complexes (Cr^{3+}, Mn^{4+})

The ground state of a free $3d^3$ ion is a ^4F atomic term, which is split by the axial LF into four orbital components, $^4F(M_L = \pm 3)$, $^4F(M_L = \pm 2)$, $^4F(M_L = \pm 1)$ and $^4F(M_L = 0)$. The $^4F(M_L = \pm 3)$ state originates from the $(xy, x2 - y2)^1(xz, yz)^1(z^2)^1$ electronic configuration. LF analysis indicates that this configuration can only occur at the $E(xy, x2 - y2) > E(xz, yz) > E(z^2)$ LF splitting pattern of 3d orbitals. Comparative LF calculations with atomic parameters $B = 650$, $C = 3000$ cm^{-1} and $\zeta = 250$ cm^{-1} for Cr^{3+} ion reveal that the orbital doublet $^4F(M_L = \pm 3)$ is the ground state when the energy difference $\Delta = E(xy, x2 - y2) - E(xz, yz)$ between the energy levels of the $(xy, x2 - y2)$ and (xz, yz) orbitals is within the range $0 \leq \Delta \leq 5850$ cm^{-1}. Beyond this range, the ground state turns to the $^4F(M_L = 0)$ orbital singlet, which is represented by a mixture of the $(xy)^1(x^2 - y^2)^1(z^2)^1$ and $(xz)^1(yz)^1(z^2)^1$ electronic configurations (Figure 3).

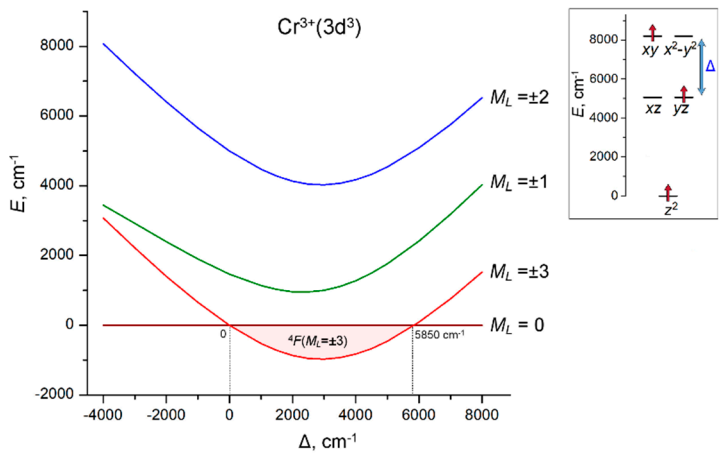

Figure 3. Dependence of the energies of the $^4F(M_L)$ LF states of $Cr^{3+}(3d^3)$ ion on the energy separation $\Delta = E(xy, x2 - y2) - E(xz, yz)$ between the $(xy, x2 - y2)$ and (xz, yz) sets of 3d orbitals. The range of the stabilization of the $^4F(M_L = \pm 3)$ ground state ($0 \leq \Delta \leq 5850$ cm^{-1}) is marked with light pink. Inset: the LF splitting pattern of 3d orbitals, $E(z^2) = 0$, $E(xz, yz) = 5000$ cm^{-1} (fixed) and $E(xy, x2 - y2) = 5000$ cm^{-1} + Δ (variable). LF calculations were done with atomic parameters $B = 650$, $C = 3000$ and $\zeta = 250$ cm^{-1}.

Evidently, the linear two-coordinate geometry of $3d^3$ complexes cannot provide the required orbital pattern $E(xy, x2 - y2) > E(xz, yz) > E(z^2)$ since linear coordination is characterized by another order of orbital energies, $E(z^2) > E(xz, yz) > E(xy, x2 - y2)$, which can result in $M_L = \pm 1$ or $M_L = \pm 2$ ground state. Therefore, unlike the record linear two-coordinate $Co^{2+}(3d^7)$ complexes with the $M_L = \pm 3$ ground state, linear $3d^3$ complexes have a maximum achievable orbital angular momentum of only $M_L = \pm 2$.

Among a variety of axial symmetry coordination geometries, the necessary orbital splitting pattern $E(xy, x2 - y2) > E(xz, yz) > E(z^2)$ can be obtained in the trigonal-prismatic coordination of the $3d^3$ ion. However, in trigonal-prismatic complexes, the energy order of 3d orbital strongly depends on the polar angle θ of the trigonal prism. In order to evaluate the conditions for stabilization of the $M_L = \pm 3$ ground state, LF calculations are performed in combination with the angular overlap model (AOM) [46–51] using the AOM parameters $e_\sigma = 9000$ cm^{-1} and $e_\sigma / e_\pi = 4$ for Cr^{3+} ions. These calculations show that the ground state

$^4F(M_L = \pm 3)$ with the maximal orbital momentum $M_L = \pm 3$ stabilizes in a compressed trigonal prism with a polar angle θ ranging between 61° and 66.5° (Figure 4a).

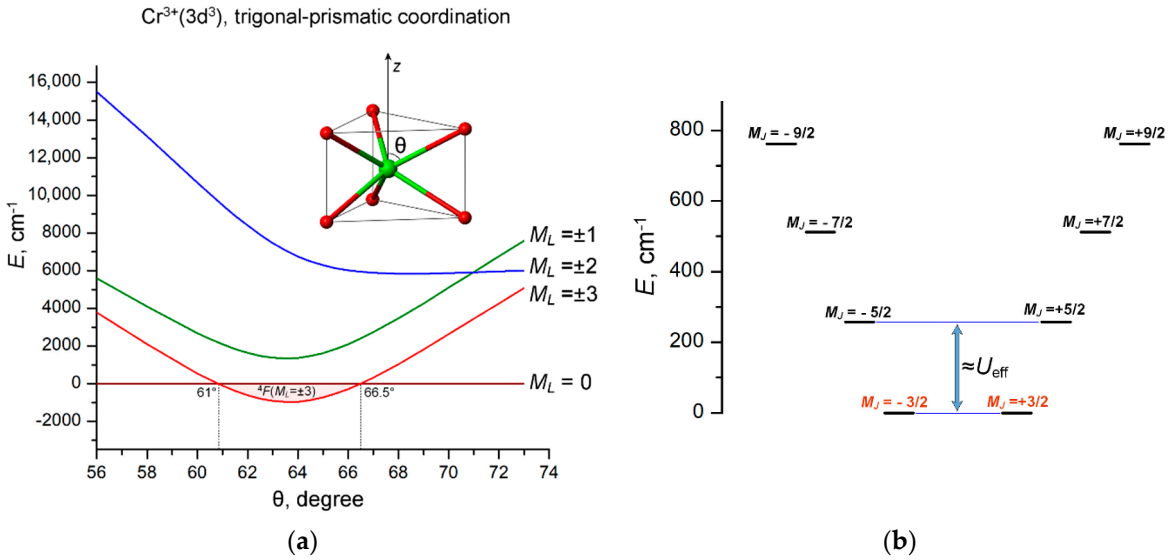

Figure 4. (**a**) Variation of the energies of the $^4F(M_L)$ LF states of $Cr^{3+}(3d^3)$ ion with increasing polar angle θ in a trigonal-prismatic coordination polyhedron. The range of the stabilization of the $^4F(M_L = \pm 3)$ ground state ($61° \leq \theta \leq 66.5°$) is marked with light pink; (**b**) E vs. M_J diagram calculated at θ = 64°. The spin-reversal barrier $U_{eff} \approx 200 = 250$ cm^{-1} is approximately estimated by the energy separation between the ground $M_J = \pm 3/2$ and the first excited $M_J = \pm 5/2$ states.

SOC splits the ground orbital doublet $M_L = \pm 3$ into four Kramer doublets with the projection of the total angular momentum $M_J = \pm 3/2$, $\pm 5/2$, $\pm 7/2$ and $\pm 9/2$, listed in order of increasing energy; their energy diagram with the total splitting energy of 762 cm^{-1} is shown in Figure 4b. These results indicate that such a complex should have a SMM behavior with a barrier of about 250 cm^{-1}, corresponding to the energy separation between the ground $M_J = \pm 3/2$ and first excited $M_J = \pm 5/2$ states. However, as opposed to linear two-coordinate Co^{II} complexes [42,43], the trigonal-prismatic $3d^3$ complexes with doubly degenerate ground state $M_L = \pm 3$ is Jahn–Teller active, subject to distortions that remove orbital degeneracy and thereby reduce the magnetic anisotropy of the complex. Nevertheless, LF/AOM calculations indicate that with moderate departures from the regular D_{3h} geometry, the overall energy pattern of the J_M states (Figure 4b) does not change much, so the trigonal-prismatic $3d^3$ complex behaves as an SMM with an estimated barrier of about 150–200 cm^{-1}.

2.3. 3d^7 Complexes (Fe^+,Co^{2+})

Linear two-coordinate $3d^7$ cobalt complex $Co^{II}(C(SiMe_2ONaph)_3)_2$ [42] is currently the only known individual mononuclear 3d complex featuring the maximal orbital angular momentum $L = 3$. From the point of view of the LF theory, in the $3d^7$ configuration the orbital LF splitting pattern $E(z^2) > E(xz, yz) > E(xy, x2 - y2)$ is a necessary condition for the stabilization of the $M_L = \pm 3$ ground state. Note that the order of the 3d orbitals in the $3d^7$ configuration is opposite to that in the $3d^3$ configuration because of the electron–hole symmetry. As in the case of $3d^2$ and $3d^3$ complexes, the additional condition is the restriction on the energy separation between the $m_l = \pm 1$ and $m_l = \pm 2$ orbitals, $\Delta = E(xz, yz) - E(xy, x2 - y2)$, which is $0 \leq \Delta \leq 6750$ cm^{-1} (Figure 5). Outside this range, the ground state is the orbital singlet $^4F(M_L = 0)$. Formally, an extra condition is a limitation on the total LF splitting energy $\Delta_{LF} = E(z^2) - E(xy, x2 - y2) < 22{,}000$ cm^{-1}, which is, however, too large to occur in a linear two-coordinate $3d^7$ complex exhibiting much lower total LF splitting energy, around 6000 cm^{-1} [42].

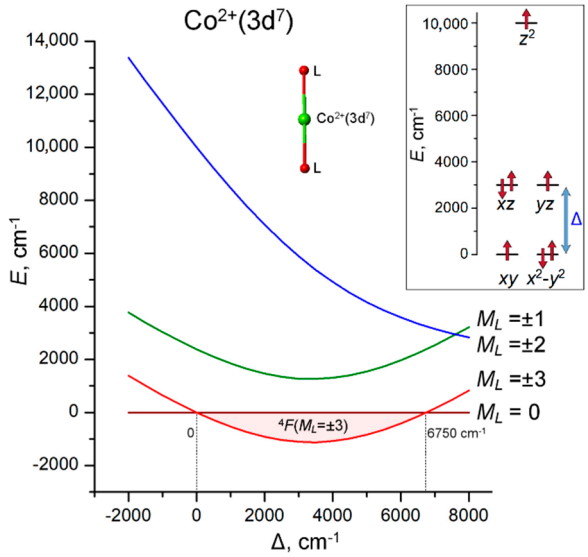

Figure 5. Energies of the $^4F(M_L)$ LF states of $Co^{2+}(3d^7)$ ion in a linear coordination as a function of the energy gap $\Delta = E(xz, yz) - E(xy, x2 - y2)$. The range of the stabilization of the $^4F(M_L = \pm 3)$ ground state ($0 \leq \Delta \leq 6750$ cm^{-1}) is marked with light pink. Inset: the LF splitting pattern of 3d orbitals, $E(xy, x2 - y2) = 0$, $E(z^2) = 10{,}000$ cm^{-1} (fixed) and $E(xz, yz) = \Delta$ (variable). LF calculations are performed with atomic parameters $B = 750$, $C = 3800$ and $\zeta = 480$ cm^{-1}.

In light of these results, it is interesting to consider the difference in the nature of the ground state of the isoelectronic linear two-coordinate $3d^7$ complexes $[Fe^{I}(C(SiMe_3)_3)_2]^-$ ($M_L = \pm 2$) [40] and $Co^{II}(C(SiMe_2ONaph)_3)_2$ ($M_L = \pm 3$) [42]. The underlying reason is the different order of the actual 3d orbitals, which is $E(xz, yz) > E(xy, x2 - y2) > E(z^2)$ (ca. 5200, 3200 and 0 cm^{-1}, respectively) in the Fe^{I} complex [40] and $E(z^2) > E(xz, yz) > E(xy, x2 - y2)$ ((ca. 5700, 3000 and 0 cm^{-1}) in Co^{II} complex [42]. A significant decrease in the energy of the $3d_{z^2}$ orbital in $Fe^{I}(C(SiMe_3)_3)_2]^-$ is caused by a very strong 4s–$3d_{z^2}$ mixing [40]. The combination of the ground orbital state $M_L = \pm 3$, the parallel coupling of the orbital momentum $L = 3$ and spin $S = 3/2$ and a sufficiently strong SOC leads to the most favorable conditions for obtaining a record spin-reversal barrier $U_{eff} = 450$ cm^{-1} of $Co^{II}(C(SiMe_2ONaph)_3)_2$ [42].

2.4. 3d^8 Complexes (Ni^{2+}, Co^{1+})

As in the case of $3d^2$ complexes with $L = 3$, the necessary condition for the occurrence of the $M_L = \pm 3$ ground state in a $3d^8$ complex is the presence of one unpaired electron on the doubly degenerate 3d orbitals with magnetic quantum numbers $m_l = \pm 1$ and $m_l = \pm 2$, i.e., $(x2 - y2, xy)^3(xz, yz)^3(z^2)^2$. For this, the order of the 3d orbitals should be the same as in $3d^3$ complexes, i.e., $E(xy, x2 - y2) > E(xz, yz) > E(z^2)$. Therefore, this LF splitting pattern can occur in trigonal-prismatic complexes (see Figure 4a), but not in linear two-coordinate complexes (Figure 5). As in the case of other above 3d complexes, there is an additional condition that constrains the energy separation between $m_l = \pm 1$ and $m_l = \pm 2$ orbitals, $\Delta = E(xy, x2 - y2) - E(xz, yz)$, which is $0 \leq \Delta \leq 7200$ cm^{-1}.(Figure 6). LF/AOM calculations for a trigonal-prismatic $3d^8$ complex with variable polar angle θ indicate that the $M_L = \pm 3$ ground state stabilizes at $61° \leq \theta \leq 74.2°$, corresponding to a compressed trigonal prism (Figure 7a). Several trigonal-prismatic cage complexes of Ni^{II} were recently reported in [52]. In these complexes, the Ni^{2+} ion is encapsulated in a frame-type clathrochelate cage, that forces robust trigonal-prismatic coordination. However, in these complexes, the polar angle θ is about 52°, which is well below the critical angle θ > 61° (Figure 7a). Accordingly, the ground state of these complexes was found to be orbital singlet $^3F(M_L = 0)$ with a second-order magnetic anisotropy due to ZFS [48], which agrees well with the results of LF/AOM calculations indicating the $M_L = 0$ ground state at $\theta \approx 52°$ (Figure 7a). One more example of a trigonal-prismatic $3d^8$ complex is given by similar

clathrochelate complexes $Co^{I}(GmCl_2)_3(BPh)_2$ reported in ref. [53]. Unfortunately, these complexes also do not fall into the range of existence of the ground state $M_L = \pm 3$ due to violation of the $\Delta > 0$ criterion (which is actually $\Delta \approx -4500$ cm^{-1}), resulting in the ground state being the orbital singlet $^3F(M_L = 0)$.

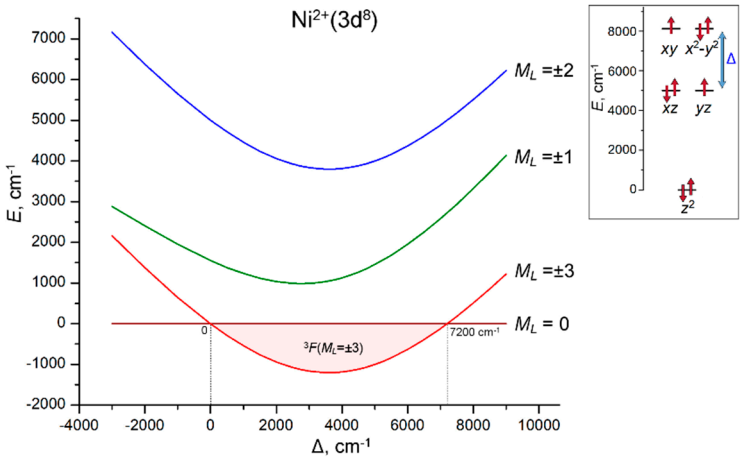

Figure 6. Variation of the energies of the $^3F(M_L)$ LF states of $Ni^{2+}(3d^8)$ ion with increasing energy gap $\Delta = E(xy, x2 - y2) - E(xz, yz)$. The range of the stabilization of the $^3F(M_L = \pm 3)$ ground state ($0 \leq \Delta \leq 7200$ cm^{-1}) is marked with light pink. Inset: the LF splitting pattern of 3d orbitals, $E(z^2) = 0$, $E(xz, yz) = 5000$ cm^{-1} (fixed) and $E(xy, x2 - y2) = 5000$ cm^{-1} + Δ (variable). LF calculations are performed with atomic parameters $B = 800$, $C = 3200$ and $\zeta = 600$ cm^{-1}.

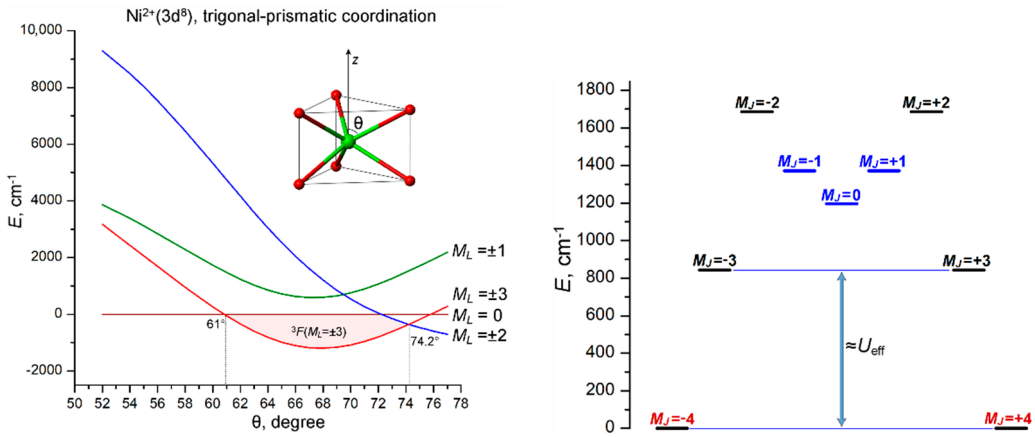

(**a**) (**b**)

Figure 7. (**a**) Variation of the energies of the $^3F(M_L)$ LF states of $Ni^{2+}(3d^8)$ ion with increasing polar angle θ in trigonal-prismatic coordination, as obtained from LF/AOM calculations. The range of the stabilization of the $^3F(M_L = \pm 3)$ ground state ($61° \leq \theta \leq 74.2°$) is marked with light pink; (**b**) E vs. M_J diagram calculated at $\theta = 64°$. The spin-reversal barrier $U_{eff} \approx 850$ cm^{-1} is approximately estimated by the energy separation between the ground $M_J = \pm 3/2$ and the first excited $M_J = \pm 5/2$ states; the $M_J = 0$ and $M_J = \pm 1$ states (marked in blue) originate from ^{2S+1}L atomic terms other than ^3F. LF/AOM calculations were performed with $e_\sigma = 5000$ cm^{-1}, $e_\sigma/e_\pi = 4$ AOM parameters and atomic parameters $B = 800$, $C = 3200$ and $\zeta = 600$ cm^{-1}.

The calculated E vs. M_J diagram suggests potentially high SMM characteristics of the compressed ($\theta > 61°$) trigonal-prismatic Ni^{2+} complex with a perfect D_{3h} symmetry. In particular, the spin-reversal barrier U_{eff}, assigned to the energy separation between the ground state $J_M = \pm 4$ and the first excited state $J_M = \pm 3$, is as high as 857 cm^{-1} (Figure 7b), which is significantly larger than in the record cobalt complex $Co^{II}(C(SiMe_2ONaph)_3)_2$

(450 cm^{-1}) [42]. However, it should be considered that, similarly to the trigonal-prismatic $3d^3$ complex, this complex is Jahn–Teller active and is subject to significant distortions that tend to reduce magnetic anisotropy. In fact, LF/AOM calculations for distorted complexes show that even subtle departures from the regular trigonal-prismatic geometry (D_{3h}) of the complex cause noticeable splitting of the ground non-Kramers doublet $J_M = \pm 4$ (tens of cm^{-1}), which should lead to complete suppression of the SMM behavior due to fast QTM processes in the split ground state $J_M = \pm 4$ (Figure 7b).

3. Materials and Methods

Ligand Field and Angular Overlap Model Calculations

Ligand-field calculations for many-electron $3d^N$ ions ($3d^2$, $3d^3$, $3d^7$ and $3d^8$) were performed in terms of the conventional LF theory involving the one-electron LF operator (specified by the set of energies of 3d orbitals in an axial LF, $E(xy, x2 - y2)$, $E(xz, yz)$ and $E(z^2)$), interelectron Coulomb repulsion (treated in terms of the Racah parameters B and C) and the spin-orbit coupling $\zeta_{3d}\Sigma_i \boldsymbol{l}_i \boldsymbol{s}_i$. Angular-overlap model calculations [46–48] for trigonal-prismatic complexes were carried out with the AOM parameters $e_\sigma = 5000$ cm^{-1} (for Ni^{2+}) and 9000 cm^{-1} (Cr^{3+}) at a fixed ratio of $e_\sigma/e_\pi = 4$. Details of LF and AOM calculations are available in the Supplementary Materials.

4. Discussion and Conclusions

This study has established that the maximum orbital angular momentum $L = 3$ observed in the linear two-coordinate $3d^7$ complex $Co^{II}(C(SiMe_2ONaph)_3)_2$ [42] (as well as in the monocoordinated Co adatom on a MgO surface [43]) is not a unique single phenomenon, but under specific conditions, it can also be obtained in some complexes of $3d^2$, $3d^3$ and $3d^8$ transition metal ions. The basic point is that in the free-ion state these ions have the ground-state atomic term ^{2S+1}F with maximal orbital angular momentum $L = 3$, which, when split in the ligand field of axial symmetry, can produce the ground orbital doublet $^{2S+1}F(M_L = \pm 3)$ with a maximum projection $M_L = \pm 3$ of the orbital momentum $L = 3$. For each of these electronic configurations, the LF splitting pattern of 3d orbitals leading to the ground orbital doublet $^{2S+1}F(M_L = \pm 3)$ has been established. Then, with the help of LF and AOM calculations, it was shown that the maximal orbital angular moment $L = 3$ is realized in the linear two-coordinate geometry for the $3d^2$ and $3d^7$ ions and in the compressed trigonal-prismatic coordination (with polar angle $\theta > 61°$) for the $3d^3$ and $3d^8$ ions. In this regard, it is worth noting that the linear two-coordinate geometry, which intuitively appears to be the most preferable for obtaining maximum magnetic anisotropy, in the case of $3d^3$ and $3d^8$ ions yields only an orbital momentum $L = 2$, not $L = 3$.

These results can be used to assess the prospects for improving the SMM performance of single-ion 3d SMMs. The calculated E vs. M_J spin energy diagrams show that the SMM performance of the linear $3d^2$ complex and the trigonal-prismatic $3d^3$ complex is significantly lower than that of the linear cobalt complex due to weaker spin-orbit coupling and antiparallel coupling of L and S. On the other hand, although the calculated spin energy diagram for the trigonal-prismatic $Ni^{2+}(3d^8)$ complex formally indicates a higher barrier ($U_{eff} \approx 850$ cm^{-1}) than for the record linear cobalt complex (450 cm^{-1}) [42], in reality, this complex is unlikely to be a good SMM because of the Jahn–Teller distortions resulting in the significant splitting of the ground non-Kramer doublet $M_J = \pm 4$ (Figure 7b), that causes fast QTM processes bypassing the barrier. Thus, despite the possible presence of maximum orbital momentum $L = 3$ in the aforementioned $3d^2$, $3d^3$ and $3d^8$ complexes, they cannot compete as SMMs with linear two-coordinate $3d^7$ cobalt complex $Co^{II}(C(SiMe_2ONaph)_3)_2$ [42].

In summary, this study has shown that the maximal orbital angular momentum $L = 3$ can occur only in $3d^2$, $3d^3$, $3d^7$ and $3d^8$ complexes with axial symmetry of the ligand field. However, the SMM performance of $3d^2$, $3d^3$ and $3d^8$ complexes appeared significantly lower than that of the linear two-coordinate $3d^7$ complex $Co^{II}(C(SiMe_2ONaph)_3)_2$ with $L = 3$. Thus, these results confirm the earlier conclusion [42] that linear two-coordinate

$3d^7$ complexes provide the maximal SMM performance of mononuclear 3d complexes (U_{eff} = 450 cm^{-1}), which is apparently near the physical limit for a single 3d metal ion.

Supplementary Materials: The following supporting information can be downloaded at: https://www.mdpi.com/article/10.3390/inorganics10120227/s1, details of LF and AOM calculations.

Author Contributions: Conceptualization, validation, methodology, writing—original draft preparation, writing—review and editing, supervision, V.S.M. All authors have read and agreed to the published version of the manuscript.

Funding: This work was supported by the Russian Science Foundation, project No. 18-13-00264.

Data Availability Statement: The data presented in this study are available in this article and in the Supplementary Materials.

Acknowledgments: V.S.M. acknowledges support by the Ministry of Science and Higher Education within the State assignment FSRC 'Crystallography and Photonics' RAS in part of the development of computational approaches for analysis of extreme magnetic anisotropy in transition-metal complexes.

Conflicts of Interest: The author declares no conflict of interest.

References

1. Sessoli, R.; Gatteschi, D.; Caneschi, A.; Novak, M.A. Magnetic bistability in a metal-ion cluster. *Nature* **1993**, *365*, 141–143. [CrossRef]
2. Gatteschi, D.; Sessoli, R. Quantum tunneling of magnetization and related phenomena in molecular materials. *Angew. Chem. Int. Ed.* **2003**, *42*, 268–297. [CrossRef] [PubMed]
3. Gatteschi, D.; Sessoli, R.; Villain, J. *Molecular Nanomagnets*; Oxford University Press: Oxford, UK, 2006. [CrossRef]
4. Leuenberger, M.N.; Loss, D. Quantum computing in molecular magnets. *Nature* **2001**, *410*, 789–793. [CrossRef] [PubMed]
5. Bogani, L.; Wernsdorfer, W. Molecular spintronics using single-molecule magnets. *Nat. Mater.* **2008**, *7*, 179. [CrossRef] [PubMed]
6. Bartolomé, J.; Luis, F.; Fernández, J.F. (Eds.) *Molecular Magnets: Physics and Applications*; NanoScience and Technology; Springer: Berlin/Heidelberg, Germany, 2014; pp. 1–395, ISBN 1010:9783642406089.
7. McInnes, E.J.L.; Winpenny, R.E.P. *4.14—Molecular Magnets. Comprehensive Inorganic Chemistry II*; Elsevier: Edinburgh, UK, 2013; Volume 4, pp. 371–396. [CrossRef]
8. Feng, M.; Tong, M.-L. Single Ion Magnets from 3d to 5f: Developments and Strategies. *Chem.—Eur. J.* **2018**, *24*, 7574–7594. [CrossRef]
9. Coronado, E. Molecular magnetism: From chemical design to spin control in molecules, materials and devices. *Nat. Rev. Mat.* **2020**, *5*, 87–104. [CrossRef]
10. Caneschi, A.; Gatteschi, D.; Lalioti, N.; Sangregorio, C.; Sessoli, R.; Venturi, G.; Vindigni, A.; Rettori, A.; Pini, M.G.; Novak, M.A. Cobalt(II)-Nitronyl Nitroxide Chains as Molecular Magnetic Nanowires. *Angew. Chem. Int. Ed.* **2001**, *40*, 1760–1763. [CrossRef]
11. Coulon, C.; Miyasaka, H.; Clérac, R. Single-Chain Magnets: Theoretical Approach and Experimental Systems. In *Single-Molecule Magnets and Related Phenomena. Structure and Bonding*; Winpenny, R., Ed.; Springer: Berlin/Heidelberg, Germany, 2006; Volume 122, pp. 163–206. [CrossRef]
12. Sun, H.-L.; Wang, Z.-M.; Gao, S. Strategies towards Single-Chain Magnets. *Coord. Chem. Rev.* **2010**, *254*, 1081–1100. [CrossRef]
13. Ishikawa, N.; Sugita, M.; Ishikawa, T.; Koshihara, S.-Y.; Kaizu, Y. Lanthanide Double-Decker Complexes Functioning as Magnets at the Single-Molecular Level. *J. Am. Chem. Soc.* **2003**, *125*, 8694–8695. [CrossRef]
14. Freedman, D.E.; Harman, W.H.; Harris, T.D.; Long, G.J.; Chang, C.J.; Long, J.R. Slow magnetic relaxation in a high-spin iron(II) complex. *J. Am. Chem. Soc.* **2010**, *132*, 1224–1225. [CrossRef]
15. Harman, W.H.; Harris, T.D.; Freedman, D.E.; Fong, H.; Chang, A.; Rinehart, J.D.; Ozarowski, A.; Sougrati, M.T.; Grandjean, F.; Long, G.J.; et al. Slow magnetic relaxation in a family of trigonal pyramidal iron(II) pyrrolide complexes. *J. Am. Chem. Soc.* **2010**, *132*, 18115–18126. [CrossRef]
16. Rinehart, J.D.; Long, J.R. Exploiting Single-Ion Anisotropy in the Design of f-Element Single-Molecule Magnets. *Chem. Sci.* **2011**, *2*, 2078–2085. [CrossRef]
17. Woodruff, D.N.; Winpenny, R.E.P.; Layfield, R.A. Lanthanide Single-Molecule Magnets. *Chem. Rev.* **2013**, *113*, 5110–5148. [CrossRef]
18. Liddle, S.T.; van Slageren, J. Improving f-Element Single Molecule Magnets. *Chem. Soc. Rev.* **2015**, *44*, 6655–6669. [CrossRef]
19. Zhang, P.; Zhang, L.; Tang, J. Lanthanide single molecule magnets: Progress and perspective. *Dalton Trans.* **2015**, *44*, 3923–3929. [CrossRef]
20. Layfield, R.; Murugesu, M. *Lanthanides and Actinides in Molecular Magnetism*; John Wiley & Sons: New York, NY, USA, 2015; pp. 1–368. ISBN 978-3-527-33526-8.
21. Lu, J.; Guo, M.; Tang, J. Recent Developments in Lanthanide Single-Molecule Magnets. *Chem.—Asian J.* **2017**, *12*, 2772–2779. [CrossRef]

22. Liu, J.-L.; Chen, Y.-C.; Tong, M.-L. Symmetry Strategies for High Performance Lanthanide-Based Single-Molecule Magnets. *Chem. Soc. Rev.* **2018**, *47*, 2431–2453. [CrossRef]
23. Feltham, H.L.C.; Brooker, S. Review of Purely 4f and Mixed-Metal nd-4f Single-Molecule Magnets Containing only One Lanthanide Ion. *Coord. Chem. Rev.* **2014**, *276*, 1–33. [CrossRef]
24. Layfield, R.A. Organometallic Single-Molecule Magnets. *Organometallics* **2014**, *33*, 1084–1099. [CrossRef]
25. Craig, G.A.; Murrie, M. 3d single-ion magnets. *Chem. Soc. Rev.* **2015**, *44*, 2135–2147. [CrossRef]
26. Frost, J.M.; Harriman, K.L.M.; Murugesu, M. The rise of 3-d single-ion magnets in molecular magnetism: Towards materials from molecules? *Chem. Sci.* **2016**, *7*, 2470–2491. [CrossRef] [PubMed]
27. Wyborne, B.G. *Spectroscopic Properties of Rare Earths*; John Wiley & Sons, Inc.: Hoboken, NJ, USA, 1965; pp. 1–241, ISBN 978-0470965078.
28. Liu, J.; Chen, Y.-C.; Liu, J.-L.; Vieru, V.; Ungur, L.; Jia, J.-H.; Chibotaru, L.F.; Lan, Y.; Wernsdorfer, W.; Gao, S.; et al. A stable pentagonal bipyramidal Dy(III) single-ion magnet with a record magnetization reversal barrier over 1000 K. *J. Am. Chem. Soc.* **2016**, *138*, 5441–5450. [CrossRef] [PubMed]
29. Ding, Y.-S.; Chilton, N.F.; Winpenny, R.E.P.; Zheng, Y.-Z. On approaching the limit of molecular magnetic anisotropy: A near-perfect pentagonal bipyramidal dysprosium(III) single-molecule magnet. *Angew. Chem. Int. Ed.* **2016**, *55*, 16071–16074. [CrossRef] [PubMed]
30. Goodwin, C.A.P.; Ortu, F.; Reta, D.; Chilton, N.F.; Mills, D.P. Molecular magnetic hysteresis at 60 kelvin in dysprosocenium. *Nature* **2017**, *548*, 439–442. [CrossRef] [PubMed]
31. Guo, F.-S.; Day, B.M.; Chen, Y.-C.; Tong, M.-L.; Mansikkamäki, A.; Layfield, R.A. Magnetic Hysteresis up to 80 Kelvin in a Dysprosium Metallocene Single-Molecule Magnet. *Science* **2018**, *362*, 1400–1403. [CrossRef]
32. Zhu, Z.; Tang, J. Lanthanide single-molecule magnets with high anisotropy barrier: Where to from here? *Natl. Sci. Rev.* **2022**, nwac194. [CrossRef]
33. Bar, A.K.; Pichon, C.; Sutter, J.-P. Magnetic Anisotropy in Two- to Eight-Coordinated Transition–Metal Complexes: Recent Developments in Molecular Magnetism. *Coord. Chem. Rev.* **2016**, *308*, 346–380. [CrossRef]
34. Boca, R. Zero-field splitting in metal complexes. *Coord. Chem. Rev.* **2004**, *248*, 757–815. [CrossRef]
35. Marriott, K.E.R.; Bhaskaran, L.; Wilson, C.; Medarde, M.; Ochsenbein, S.T.; Hill, S.; Murrie, M. Pushing the limits of magnetican-isotropy in trigonal bipyramidal Ni(II). *Chem. Sci.* **2015**, *6*, 6823–6828. [CrossRef]
36. Novikov, V.V.; Pavlov, A.A.; Nelyubina, Y.V.; Boulon, M.-E.; Varzatskii, O.; Voloshin, Y.Z.; Winpenny, R.E.P. A Trigonal Prismatic Mononuclear Cobalt(II) Complex Showing Single-Molecule Magnet Behavior. *J. Am. Chem. Soc.* **2015**, *137*, 9792–9795. [CrossRef]
37. Yao, B.; Singh, M.K.; Deng, Y.-F.; Wang, Y.-N.; Dunbar, K.R.; Zhang, Y.-Z. Trigonal Prismatic Cobalt(II) Single-Ion Magnets: Manipulating the Magnetic Relaxation Through Symmetry Control. *Inorg. Chem.* **2020**, *59*, 8505–8513. [CrossRef]
38. Sutter, J.P.; Béreau, V.; Jubault, V.; Bretosh, K.; Pichon, C.; Duhayon, C. Magnetic anisotropy of transition metal and lanthanide ions in pentagonal bipyramidal geometry. *Chem. Soc. Rev.* **2022**, *51*, 3280–3313. [CrossRef]
39. Zadrozny, J.M.; Atanasov, M.; Bryan, A.M.; Lin, C.-Y.; Rekken, B.D.; Power, P.P.; Neese, F.; Long, J.R. Slow magnetization dynamics in a series of two-coordinate iron(II) complexes. *Chem. Sci.* **2013**, *4*, 125–138. [CrossRef]
40. Zadrozny, J.M.; Xiao, D.J.; Atanasov, M.; Long, G.J.; Grandjean, F.; Neese, F.; Long, J.R. Magnetic blocking in a linear iron(I) complex. *Nat. Chem.* **2013**, *5*, 577–581. [CrossRef]
41. Yao, X.-N.; Du, J.-Z.; Zhang, Y.-Q.; Leng, X.-B.; Yang, M.-W.; Jiang, S.-D.; Wang, Z.-X.; Ouyang, Z.-W.; Deng, L.; Wang, B.-W.; et al. Two-Coordinate Co(II) Imido Complexes as Outstanding Single-Molecule Magnets. *J. Am. Chem. Soc.* **2017**, *139*, 373–380. [CrossRef]
42. Bunting, P.C.; Atanasov, M.; Damgaard-Møller, E.; Perfetti, M.; Crassee, I.; Orlita, M.; Overgaard, J.; van Slageren, J.; Neese, F.; Long, J.R. A linear cobalt(II) complex with maximal orbital angular momentum from a non-Aufbau ground state. *Science* **2018**, *362*, eaat7319. [CrossRef]
43. Rau, G.; Baumann, S.; Rusponi, S.; Donati, F.; Stepanow, S.; Gragnaniello, L.; Dreiser, J.; Piamonteze, C.; Nolting, F.; Gangopadhyay, S.; et al. Reaching the magnetic anisotropy limit of a 3d metal atom. *Science* **2014**, *344*, 988–992. [CrossRef] [PubMed]
44. Powell, P.P. Stable Two-Coordinate, Open-Shell (d^1–d^9) Transition Metal Complexes. *Chem. Rev.* **2012**, *112*, 3482–3507. [CrossRef]
45. Reber, C.; Güdel, H.U. Near-infrared luminescence spectroscopy of Al_2O_3:V^{3+} and YP_3O_9:V^{3+}. *Chem. Phys. Lett.* **1989**, *154*, 425–431. [CrossRef]
46. Schaeffer, C.E.; Jorgensen, C.K. The angular overlap model, an attempt to revive the ligand field approaches. *Mol. Phys.* **1965**, *9*, 401–412. [CrossRef]
47. Schäffer, C.E. A perturbation representation of weak covalent bonding. *Struct. Bonding.* **1968**, *5*, 68–95. [CrossRef]
48. Jorgensen, C.K. The Nephelauxetic Series. *Prog. Inorg. Chem.* **1962**, *4*, 73–124. [CrossRef]
49. Mironov, V.S.; Bazhenova, T.A.; Manakin, Y.V.; Lyssenko, K.A.; Talantsev, A.D.; Yagubskii, E.B. A new Mo(IV) complex with the pentadentate (N_3O_2) Schiff-base ligand: The first non-cyanide pentagonal–bipyramidal paramagnetic 4d complex. *Dalton Trans.* **2017**, *46*, 14083–14087. [CrossRef] [PubMed]
50. Manakin, Y.V.; Mironov, V.S.; Bazhenova, T.A.; Lyssenko, K.A.; Gilmutdinov, I.F.; Bikbaev, K.S.; Masitov, A.A.; Yagubskii, E.B. $(Et_4N)[Mo^{III}(DAPBH)Cl_2]$, the first pentagonal-bipyramidal Mo(III) complex with a N_3O_2-type Schiff-base ligand: Manifestation of unquenched orbital momentum and Ising-type magnetic anisotropy. *Chem. Commun.* **2018**, *54*, 10084–10087. [CrossRef]

51. Bazhenova, T.A.; Zorina, L.V.; Simonov, S.V.; Mironov, V.S.; Maximova, O.V.; Spillecke, L.; Koo, C.; Klingeler, R.; Manakin, Y.V.; Vasiliev, A.N.; et al. The first pentagonal-bipyramidal vanadium(iii) complexes with a Schiff-base N_3O_2 pentadentate ligand: Synthesis, structure and magnetic properties. *Dalton Trans.* **2020**, *49*, 15287–15298. [CrossRef]
52. Campanella, A.J.; Ozvat, T.M.; Zadrozny, J.M. Ligand design of zero-field splitting in trigonal prismatic Ni(ii) cage complexes. *Dalton Trans.* **2022**, *51*, 3341–3348. [CrossRef]
53. Nehrkorn, J.; Veber, S.L.; Zhukas, L.A.; Novikov, V.V.; Nelyubina, Y.V.; Voloshin, Y.Z.; Holldack, K.; Stoll, S.; Schnegg, A. Determination of Large Zero-Field Splitting in High-Spin Co(I) Clathrochelates. *Inorg. Chem.* **2018**, *57*, 15330–15340. [CrossRef]